Materials Chemistry and Physics 139 (2013) 817–824

Contents lists available at SciVerse ScienceDirect

Materials Chemistry and Physics

journal homepage: www.elsevier.com/locate/matchemphys

# Phosphate ions as inhibiting agents for copper corrosion in chlorinated tap water

L. Yohai [a], W.H. Schreiner [b], M. Vázquez [a,*], M.B. Valcarce [a]

[a] División Electroquímica y Corrosión, INTEMA, CONICET, UNMdP, Juan B. Justo 4302, B7608FDQ Mar del Plata, Argentina
[b] Laboratório de Superfícies e Interfases, Departamento de Física, Universidade Federal do Paraná, 81531-990 Curitiba, PR, Brazil

## HIGHLIGHTS

- ► Changes in the copper corrosion after adding phosphate to tap water were analyzed.
- ► When NaClO and phosphates are present, $Cu_3(PO_4)_2$ participates of the surface film.
- ► In the absence of biocide the surface film contains a mixture of $Cu_2O$, CuO and $Cu(OH)_2$.
- ► $PO_4^{3-}$ is an effective inhibitor for Cu in tap water containing high NaClO dosages.

## ARTICLE INFO

*Article history:*
Received 22 October 2012
Received in revised form
17 January 2013
Accepted 12 February 2013

*Keywords:*
Surfaces
Electrochemical techniques
Raman spectroscopy and scattering
X-ray photo-emission spectroscopy (XPS)

## ABSTRACT

$PO_4^{3-}$ ions as corrosion inhibitor were investigated on copper in tap water in the presence of NaClO. The inhibitor was evaluated by electrochemical techniques and weight loss tests. Raman spectroscopy and X-ray photoelectron spectroscopy were used to study the passive layer. In inhibited tap water, the passive layer is thick and compact if NaClO is present. Weight-loss tests showed the inhibition of uniform dissolution and no pitting attack. When adding NaClO, $Cu_3(PO_4)_2$ is incorporated to the passive film. Thus, phosphate ions are effective as inhibitors for copper in tap water, even when using high dosages of biocides.



## 1. Introduction

Copper and copper alloys are materials largely used in tap water distribution systems where sodium hypochlorite is frequently used as biocide to reduce the bacterial content. As a side effect, this biocide could increase copper corrosion, favouring the $Cu^{2+}$ release to the water, even inducing the development of localized corrosion depending on the tap water composition and the chlorine content [1–4]. Hypochlorite reduction is the dominant cathodic reaction in chlorinated tap water (instead of oxygen reduction), shifting the corrosion potential above the pitting potential. Also, sodium hypochlorite stimulates pit growth [4,5].

Corrosion inhibitors are widely used to prevent copper dissolution. In the context of this work, the inhibitors should be harmless for human health and friendly with the environment [6]. Sodium orthophosphate fulfils these requirements. In fact, the beneficial effect of phosphates ions on copper in a variety of tap water compositions, in relation with copper release rate into water, has been studied by many authors [7–14] However, the action mechanism of this inhibitor is not clearly understood. It has been suggested that it lowers copper solubility, forming a cupric phosphate layer on the copper surface [7,15]. When the electrolyte composition and pH allow the development of a superficial protective layer on the metal, $Cu^{2+}$ release to the medium is minimal. However, this layer can suffer localized rupture or pitting that can lead to pipe perforation. In previous works [16–18] we established that in a hard and highly carbonated tap water, sodium orthophosphate can be used as corrosion inhibitor, as it favours the development of a more resistant superficial layer that minimizes copper dissolution. It also acts by decreasing the susceptibility to localized corrosion. In these studies the optimal dosage of inhibitor was established. Also, an inhibition mechanism of phosphate ions on copper in tap water was presented, showing that in this case CuO was the principal component of the passive layer (instead of a cupric phosphate). In agreement with these results, Lytle and Nadagouda [13] have recently presented an analysis of copper pipes from drinking water plumbing in USA suggesting that phosphate ions in tap water are important in preventing pitting corrosion of copper in actual service conditions.

* Corresponding author. División Electroquímica y Corrosión, INTEMA, Facultad de Ingeniería, UNMdP, Juan B. Justo 4302, B7608FDQ Mar del Plata, Argentina. Tel.: +54 223 481 6600; fax: +54 223 481 0046.
*E-mail address:* mvazquez@fi.mdp.edu.ar (M. Vázquez).

0254-0584/$ – see front matter © 2013 Elsevier B.V. All rights reserved.
http://dx.doi.org/10.1016/j.matchemphys.2013.02.037

This investigation has been carried out employing a solution that simulates Mar del Plata drinkable water. This is a seaside city in Argentina (lat. S:3756 – long. W:5735), where the source for tap water is underground wells. This water is moderately hard and highly carbonated. Due to the intrusion of the marine aquifers, the chloride ions content is relatively high for international standards and never less than 2.82 mmol $l^{-1}$ (100 mg $l^{-1}$). Argentine food-grade norms set the upper limit for chloride ions content in 10 mmol $l^{-1}$ for safe drinking water [19].

The effect of orthophosphate ions as corrosion inhibitor of copper in tap water, when sodium hypochlorite is also present, is controversial and there are very few papers that deal with this issue [9,14,20]. The inhibitor effects on pitting corrosion and its action mechanism could be affected by the presence of sodium hypochlorite. In this context, the combined effect of orthophosphate ions and sodium hypochlorite on copper corrosion inhibition in tap water is studied. Particular attention will be paid to the composition of the surface film naturally formed on copper in contact with water containing both the inhibiting agent (phosphate ions) and sodium hypochlorite as biocide. The effect of each species on the protection mechanism will be evaluated.

## 2. Materials and methods

### 2.1. Electrodes preparation

The electrodes were constructed from spectroscopic grade copper (99.99%). Disc samples of copper were included in fast curing acrylic resin on appropriated polyvinyl chloride (PVC) holders. The geometrical area exposed was 0.312 $cm^2$. An appropriated electrical contact was prepared for each sample. The electrodes were abraded down to grade 600 with emery paper, and finally mirror polished with 0.05 μm alumina powder (Type B – Buehler, Lake Bluff, USA). The electrodes were then rinsed gently with distilled water.

In the case of weight loss tests, copper coupons were abraded only up to grade 600 with emery paper. The exposed geometrical area was 2.1 $cm^2$.

### 2.2. Electrolyte composition

The experiments were carried out using artificial tap water (ATW) simulating the average composition of the drinkable water of an Argentine coastal city. The mineral base composition was $MgSO_4 \cdot 7H_2O$ (0.163 mmol $l^{-1}$), $MgCl_2 \cdot 6H_2O$ (0.295 mmol $l^{-1}$), $KNO_3$ (0.247 mmol $l^{-1}$), $CaCl_2 \cdot H_2O$ (0.853 mmol $l^{-1}$), $Na_2CO_3$ (4.43 mmol $l^{-1}$) and $NaNO_3$ (0.235 mmol $l^{-1}$) in distilled water; the pH was adjusted to 7.6 with 1 mol $l^{-1}$ HCl. The final water conductivity was 1.15 mS $cm^{-1}$. The final chloride ions concentration determined by potentiometric titration was 5.6 mmol $l^{-1}$.

To evaluate the inhibitor effect, the dosage of orthophosphate tested corresponds to 0.32 mmol $l^{-1}$ $NaH_2PO_4 \cdot H_2O$ respectively. A stock solution containing 0.05 g $ml^{-1}$ $NaH_2PO_4 \cdot H_2O$ was used (equivalent to 0.36 mol $l^{-1}$). The solutions containing the inhibitor will be identified as IATW.

To analyze the role played by NaClO as biocide, a commercial bleach solution provided by Química DEM™ was used as stock. The NaClO concentration in the commercial solution was evaluated by titration [21]. In the experiments to be described below, two NaClO dosages were used: 0.056 and 0.14 mmol $l^{-1}$. These relatively high dosages correspond to 2 and 5 mg $l^{-1}$ expressed as $Cl_2$, respectively. The World Health Organization recommends a maximum value of 5 mg $l^{-1}$ for free chlorine in drinking-water [22]. The highest dosage of biocide was only used in phosphate-free ATW when performing weight-loss tests. These solutions will be referred to as ATW-BH. On the other hand, the lowest dosage of NaClO (0.056 mmol $l^{-1}$) as biocide was used in phosphate-free ATW for the rest of the electrochemical tests. These solutions will be referred to as ATW-BL. The solutions containing both, the inhibitor and the biocide, will be denoted as IATW-BH. In this case, the NaClO dosage is always 0.14 mmol $l^{-1}$.

All the experiments were carried out at room temperature (20 ± 2 °C). The solutions were used without stirring or deareation, unless otherwise noted.

### 2.3. Electrochemical techniques

A three-electrode electrochemical cell was used. A saturated calomel electrode (SCE, $E$ = 0.24 V vs. the standard hydrogen electrode, SHE) was used as reference. All the potentials were indicated against SCE. A platinum wire of large area was used as counter electrode. A Luggin capillary minimized the ohmic drop.

A Voltalab PGZ 100 potentiostat was used to carry out the electrochemical characterization.

Before all the electrochemical tests, the copper electrodes were pre-reduced in ATW at −1.15 $V_{SCE}$ for 15 min to obtain a reproducible, clean surface.

Polarization resistance ($R_p$) was evaluated as $\Delta V/\Delta i$, from potential sweeps scanning ±10 mV from the corrosion potential ($E_{corr}$) at a scan rate of 0.1 mV $s^{-1}$. The electrodes had been previously kept at $E_{corr}$ for 2 h.

Film growth was investigated carrying out potentiodynamic reductions. First, the passive film was grown at the corrosion potential ($E_{corr}$) for 2 h. Then the electrodes were immediately transferred to another cell where the oxides were reduced in deareated ATW by scanning the potential at 10 mV $s^{-1}$. The starting point was the potential where the oxide had been grown. The potential was scanned in the negative direction up to −1.15 $V_{SCE}$.

When anodic polarization curves were registered, the electrodes were first kept at $E_{corr}$ for 2 h. The passive layer was then stable and the open circuit potential remained constant. Finally a potentiodynamic scan started at the $E_{corr}$, using a sweep rate of 0.1 mV $s^{-1}$. To induce a convenient degree of attack, the scan direction was reversed at 0.64 mA $cm^{-2}$. The overall procedure followed the recommendations of ASTM [23], adapted for copper.

Electrochemical impedance spectroscopy (EIS) tests were performed at $E_{corr}$. Recording each spectrum took between 90 and 160 min. Prior to starting the frequency sweep, the samples were pretreated for 15 min at −1.15 $V_{SCE}$ and then kept for 2 h in contact with ATW at $E_{corr}$. The amplitude of the AC voltage signal was ±10 $mV_{rms}$ while the frequency varied between 20 kHz and 5 mHz.

### 2.4. Ex-situ Raman spectra

Ex-situ Raman spectra were performed on the passive layers on copper grown for 192 h at $E_{corr}$. The samples were then cleaned with de-ionized water and dried with ethylic alcohol under nitrogen current. Raman spectra were collected at various points (al least five), and were found to produce similar results.

The Raman measurements were carried out using an Invia Reflex confocal Raman microprobe with $Ar^+$ laser of 514 nm in backscattering mode, with a laser spot of 2 μm. An exposure time of 50 s and 3 accumulations were used, with 50× objective. The laser power was 25 mW.

### 2.5. XPS spectroscopy

The films on copper were prepared as described above (Section 2.4) and immediately introduced into the XPS chamber. The XPS spectra were performed using an XPS VG Microtech ESCA3000 (MgKα and AlKα radiations) at an operating pressure of $3.10^{-10}$ mbar.

All XPS spectra are acquired at 45° between the analyzer axis and the sample surface normal set. Survey spectra were recorded for the samples in the 0–1100 eV binding energy range, using 1 eV steps and a bandpass of 50 eV (not shown). High resolution scans with 0.1 eV steps and bandpass of 20 eV were conducted over the regions of interest. In every case, surface charging effects were compensated by referencing the binding energy (BE) to the C 1s line of residual carbon set at 284.5 eV BE [24]. The composite XPS bands were resolved using XI SDP32 software, version 3.0.

### 2.6. Weight loss determinations

Previously weighted coupons were suspended and immersed in the following test solutions: ATW, ATW-BH, IATW and IATW-BH. Each container held three coupons. The containers were kept at room temperature in aerated conditions, in the darkness to avoid NaClO degradation. Every 2 days, the solutions were partially replaced in order to keep the NaClO level constant. The coupons were withdrawn after 90 days and the corrosion products were stripped by immersion in 1 mol $l^{-1}$ HCl. Then the coupons were neutralized and rinsed, first with a saturated $Na_2CO_3$ solution, and finally with distilled water.

## 3. Results and discussion

The polarization resistance values ($R_p$) measured in ATW, ATW-BL and IATW-BH after 2 h at the $E_{corr}$ are displayed in Table 1. In the absence of phosphate ions, NaClO concentrations higher than 0.056 mmol $l^{-1}$ are too aggressive for the copper surface. From Table 1 it can be seen that copper in ATW-BL presents lower $R_p$ values and a more negative $E_{corr}$ than in ATW. In IATW-BH, $E_{corr}$ moves towards more noble potentials with a notorious increase in the $R_p$ values. The positive effect of phosphate ions is evident, even when the NaClO content is over twice higher than in the reference condition. The augmentation in $E_{corr}$ and $R_p$ observed when NaClO and the inhibitor are present together could be associated to NaClO reduction [4,5], and to differences in the composition of the protective passive layer developed on the copper surface.

Fig. 1 shows potentiodynamic reduction curves of the layers grown during 2 h at the $E_{corr}$ in ATW, IATW and IATW-BH. In ATW, peak IIc at −0.74 $V_{SCE}$ has been associated to $Cu_2O$ reduction to Cu and the shoulder at −0.95 $V_{SCE}$ (IIIc) to the reduction of Cu(I) in solution [16,25,26]. In the presence of the inhibitor, a new cathodic peak at −0.35 $V_{SCE}$ (Ic') appears, related to the presence of CuO and its reduction to $Cu_2O$ [16,17]. Peak II'c at −0.57 $V_{SCE}$ can be associated to $Cu_2O$ reducing to Cu [16,17]. The charge ($q$) associated to peaks IIc in ATW, and I'c and II'c in IATW, has been calculated by current integration. The relation to the total charge is $q_{IATW}/q_{ATW} = 0.43$ indicating the development a thinner passive layer once the inhibitor is present [16]. When the inhibitor and the biocide are both present, the reduction charge increases (Ic" and IIc") and the relation to the total charge is now $q_{IATW\text{-}BH}/q_{ATW} = 0.98$ indicating the presence of a thicker passive layer.

Impedance spectra are recorded on copper held 2 h at $E_{corr}$ in ATW, ATW-BL, IATW and IATW-BH. A schematic representation of the structure of the surface film present on the metallic surfaces after ageing, as well as the corresponding equivalent circuit showing the best fitting results, are presented in Fig. 2. This circuit

**Table 1**
Polarization resistance values obtained after growing surface layer at $E_{corr}$ for 2 h.

| | ATW-BL | ATW | IATW | IATW-BH |
|---|---|---|---|---|
| $E_{corr}$ ($mV_{SCE}$) | −90 ± 62 | −59 ± 15 | −72 ± 15 | 78 ± 17 |
| $R_p$ (kΩ $cm^2$) | 11 ± 4 | 33 ± 10 | 96 ± 4 | 221 ± 36 |

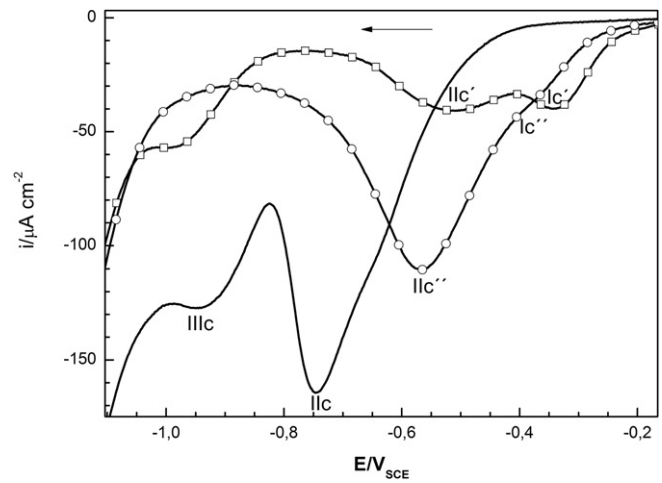


**Fig. 1.** Potentiodynamic reduction curves for copper oxides grown during 2 h at $E_{corr}$ in ATW (—); IATW (—□—), IATW-BH (—○—). Scan rate: 10 mV $s^{-1}$.

includes constant phase elements (CPE) to represent various types of non homogeneities typical of corroding electrodes. Surface roughness, insufficient polishing, grain boundaries and surface impurities have been mentioned before among the main reasons that justify the use of CPEs in equivalent circuits of corroding electrodes [27]. The impedance of this element is frequency-dependent, and can be mathematically expressed using two parameters, $Q$ and $n$ as:

$$Z_{CPE} = \left[Q(j\omega)^n\right]^{-1} \quad (1)$$

where $Q$ is a constant with dimensions of $\Omega^{-1}$ $cm^{-2}$ $s^n$ and $n$ a constant power, with $-1 < n < 1$. A rough or porous surface can cause a double layer capacitance to appear as a constant phase element with $n$ varying between 0.5 and 1. Warburg impedances and CPEs with a $n$ value around 0.5 (the last known as "infinite diffusion") are used to model surface layers with increasing ionic conductivity due to corrosion processes occurring inside the pores, and the consequent diffusion process along them. This circuit is typical of passive metals and has been used before by other authors in relation to copper corrosion in tap water [26,28,29]. $R_s$ represents the solution resistance between the electrode surface and the tip of

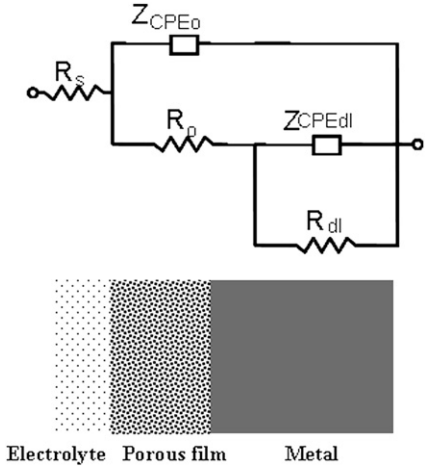


**Fig. 2.** Equivalent circuit proposed to fit the experimental data when two time constants are present. $R_s$ represents the solution resistance, $Z_{CPEo}$ the pseudo-capacitance of the surface oxide, $R_o$ the electrolyte resistance in the pores of the oxide film, $Z_{CPEdl}$ the pseudo-capacitance of the double layer and $R_{dl}$ the double layer resistance.

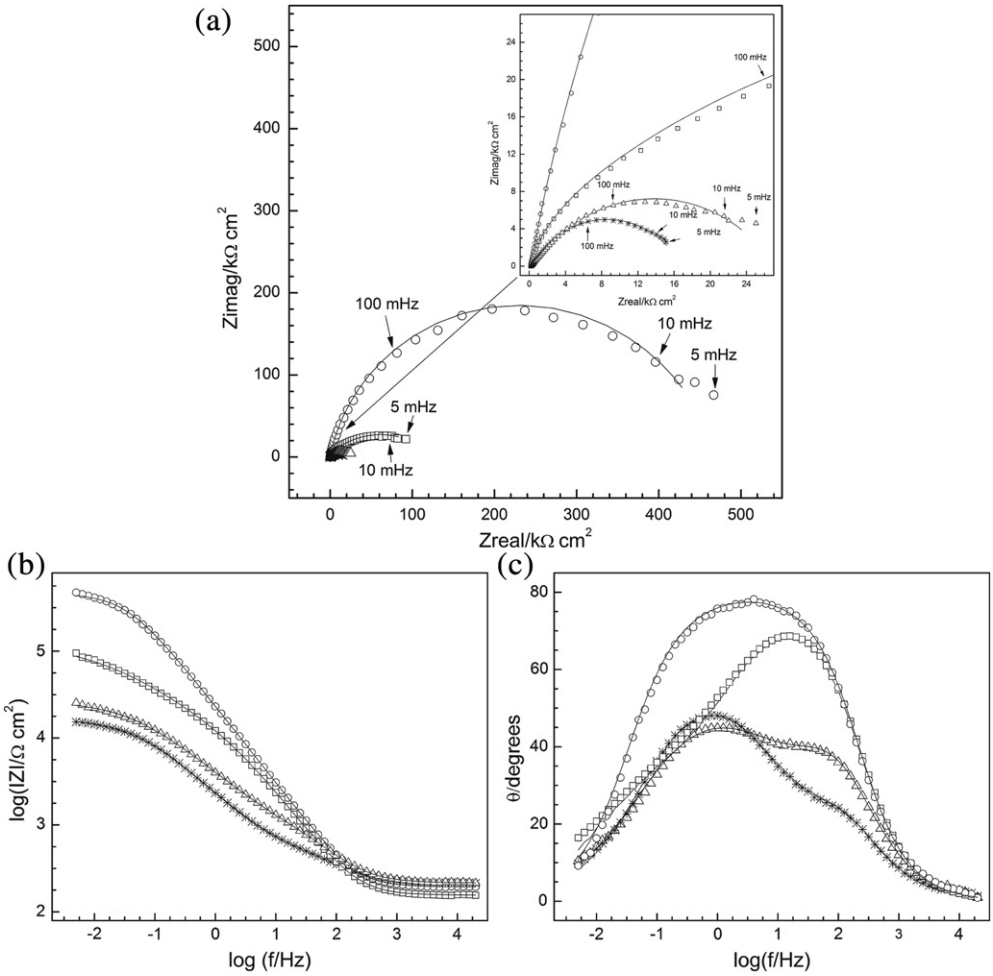


**Fig. 3.** Impedance spectra recorded on copper electrodes held for 2 h at $E_{corr}$ in ATW (—Δ—), ATW-BL (—*—), IATW (—□—), IATW-BH (—○—). The symbols represent the data and the lines the fitting results. (a) Nyquist representation; (b) and (c) Bode representation.

the Luggin capillary, $Z_{CPEo}$ a constant related to the surface oxide, $R_o$ represents the electrolyte resistance in the pores of the oxide film, $Z_{CPEdl}$ is a constant related to the double layer and $R_{dl}$ the double layer resistance. The experimental data were fitted to the proposed equivalent circuit using ZView™ [30].

The results are shown in Fig. 3 in the form of Nyquist (a) and Bode (b and c) plots. EIS data fit results are shown together with the recorded data. As can be seen, the impedance spectra present two time constants. The use of the same equivalent circuit with and without inhibitor is in agreement with the presence of two time constants in all the conditions analyzed. The first time constant at high frequency is associated to the presence of a passive film and the second time constant to low frequency is associated to the charge transference resistance process at the metal/film interface. In ATW and ATW-BL the two time constants can be easily appreciated in Fig. 3c. In the case of IATW the presence of the two time constants may not be so evident. However, the lack of symmetry in the Bode plot indicates the presence of two overlapped time constants [16]. In IATW-BH the Bode plot presents a plateau in

**Table 2**
Optimized values for the parameters employed in fitting the data in Fig. 3a, b and c with the equivalent circuit proposed in Fig. 2.

| Element | ATW-BL | ATW | IATW | IATW-BH |
|---|---|---|---|---|
| $R_s$/Ω cm² | 213 | 214 | 155 | 194 |
| $Q_o$/μΩ$^{-1}$ cm$^{-2}$ s$^n$ | 23.4 | 13.8 | 10.5 | 8.2 |
| $n_o$ | 0.80 | 0.82 | 0.88 | 0.89 |
| $R_o$/kΩ cm² | 0.4 | 1.0 | 12.9 | 216.6 |
| $Q_{dl}$/μΩ$^{-1}$ cm$^{-2}$ s$^n$ | 104.3 | 69.0 | 30.1 | 2.2 |
| $n_{dl}$ | 0.68 | 0.61 | 0.5 (fixed) | 0.5 (fixed) |
| $R_{dl}$/kΩ cm² | 16.1 | 25.9 | 112.7 | 259.1 |

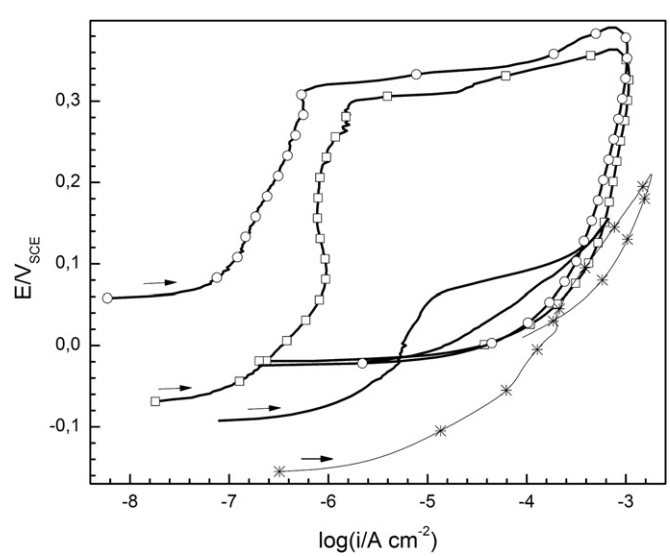


**Fig. 4.** Anodic polarization curves for copper after 2 h at $E_{corr}$ in ATW (—), ATW-BL (—*—), IATW (—□—), IATW-BH (—○—). Scan rate: 0.1 mV s$^{-1}$.

**Table 3**
Electrochemical parameters obtained from anodic polarization curves for copper.

| | ATW-BL | ATW | IATW | IATW-BH |
|---|---|---|---|---|
| $E_{pit}$ ($mV_{SCE}$) | – | 71 ± 13 | 277 ± 49 | 326 ± 13 |
| $E_{pit} - E_{corr}$ (mV) | – | 130 ± 28 | 348 ± 54 | 249 ± 15 |

the range of frequencies where the two time constants are observed in the other conditions, indicating also the presence the two overlapped time constants.

The experimental data are found to reasonably fit the proposed equivalent circuit. When the inhibitor is added to ATW, $n_{dl}$ is fixed at 0.5 during the fitting procedure to simulate a Warburg element. The low frequency time constant is therefore associated to diffusion impedance combined with a charge transfer process. In the present case, the diffusion impedance could represent the hindered diffusion of $Cu^+$ through the less porous passive layer [26,41]. The optimized parameter values are presented in Table 2. When 0.056 mmol $l^{-1}$ NaClO are present in ATW, a decrease of $R_o$ and $R_{dl}$, together with an increase of $Q_o$ and $Q_{dl}$, can be associated to the presence of a more porous passive layer on the electrode surface when compared to ATW. When the inhibitor and the biocide are present simultaneously, $Q_o$ shows no relevant variation relative to ATW, but $Q_{dl}$ decreases. This behaviour, together with an increment of $R_o$ and $R_{dl}$, indicates the development of a more compact passive layer, as compared to ATW [28]. The increment of $n_o$ up to values close to 0.9 is related to a more capacitive response associated to a less porous surface [31].

Anodic polarization curves are presented in Fig. 4 for copper in ATW, ATW-BL, IATW and IATW-BH. Table 3 presents average values for the pitting potential ($E_{pit}$), taken from at least three independent experiments. $E_{pit}$ is taken as the potential where the current increases abruptly.

Images showing the status of the surface after having performed the anodic polarization curves are presented in Fig. 5. All the conditions produce pitting attack, except for ATW with NaOCl, where corrosion is predominantly uniform. In this case, the current increases steadily and there is no clear passivity current (Fig. 4).

In the two conditions where the inhibitor is present, it can be seen that the pitting potential moved in the direction of more positive (noble) values while the passivity currents decreased and the difference ($E_{pit} - E_{corr}$) increased. This better pitting resistance when the inhibitor is added to ATW or ATW with NaClO, may be attributed to the presence of a more protective surface layer. As it can be seen in Fig. 5, the highest density of pits corresponds to IATW-BH and the lowest to IATW. However, in IATW the pits are bigger and deeper. The differences in the morphology of attack could be related to changes in the composition of the passive layer when NaClO is present.

To complete the surface characterization, ex-situ Raman and XPS techniques were used in order to compare the effect of $PO_4^{3-}$ ions on copper. To enable the development of a thicker passive layer, these films were grown at $E_{corr}$ for a longer time (192 h).

Raman spectroscopy provides direct information on the bonding, composition and stoichiometry of both crystalline and amorphous surface compounds on metals [32]. Ex-situ Raman spectra of the passive layers grown on copper in ATW, IATW and IATW-BH are presented in Fig. 6. In ATW, narrow and intense bands at 150 and 220 $cm^{-1}$ together with a broad feature in the frequency range from 300 a 700 $cm^{-1}$ show that the oxide layer is mainly composed by $Cu_2O$ [33,34]. CuO cannot be identified because the Raman scattering from CuO is much weaker than that from $Cu_2O$. Also, the main peak in the CuO spectrum lies too close to one of the most intense $Cu_2O$ peaks. When the inhibitor is added, a decrease in the intensity of the Raman signal is evident. This fact could be associated to the presence of $Cu_2O$ and CuO on the surface film,

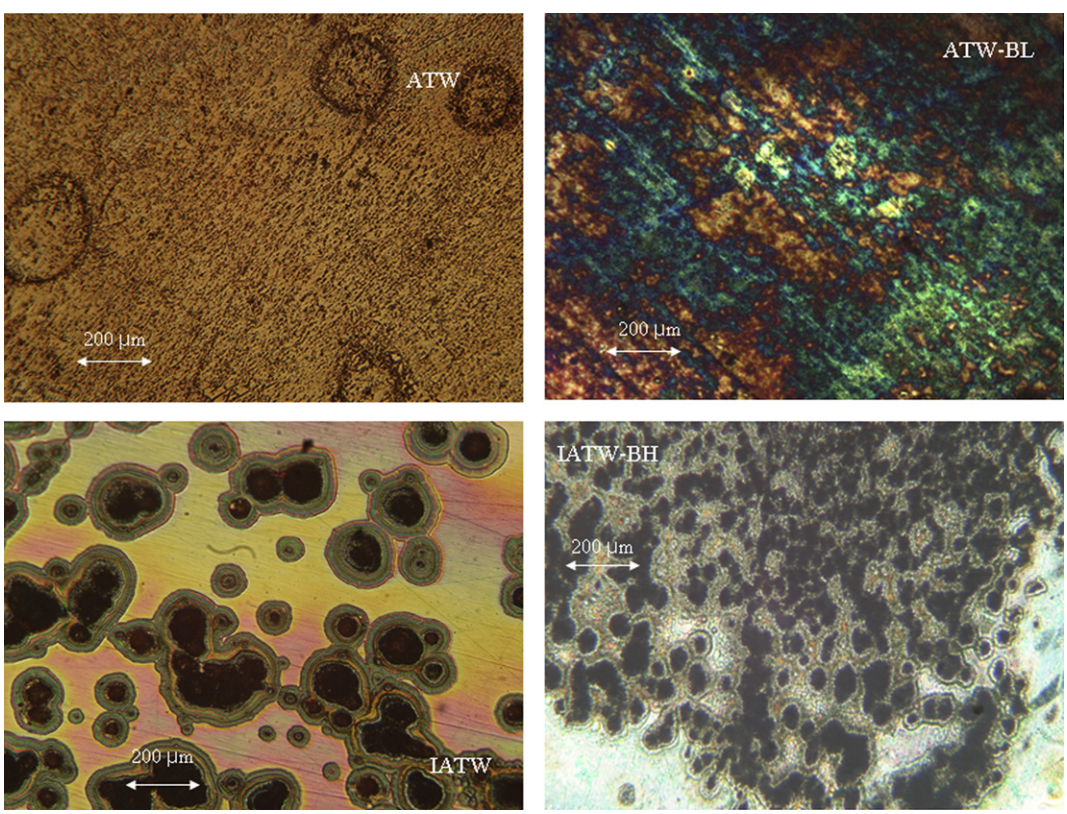


**Fig. 5.** Micrographs of the electrodes surface after performing anodic polarization curves.

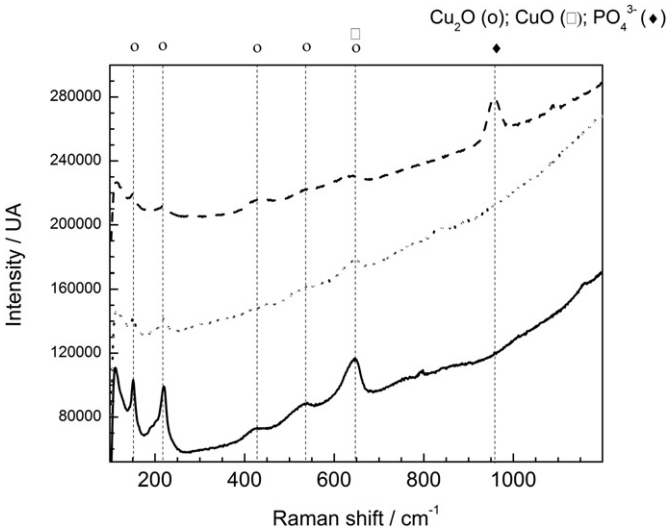


**Fig. 6.** Raman spectra for passive layers grown on copper for 192 h at $E_{corr}$ in ATW (—); IATW (···) and IATW-BH (—·—).

because the scattering from $Cu_2O$, diluted by CuO, has been reported to be much weaker than that from pure $Cu_2O$ [17,33]. In the presence of NaClO and $PO_4^{3-}$ the participation of $Cu_3(PO_4)_2$ on the surface film on copper is evidenced by the intense band that appears at 960 $cm^{-1}$ [35–38]. This band can be ascribed to the symmetric stretching mode ($\nu_1$) of $PO_4^{3-}$ ions [37–39].

XPS spectra were recorded for passive layers grown on copper in IATW and IATW-BH. The Cu2p region for both materials is presented in Fig. 7. In the case of $Cu_2O$, the $Cu2p_{3/2}$ peak is located at a binding energy of 932.2–932.8 eV [24,40,41], close to the metallic copper signal. By means of XPS, CuO and $Cu(OH)_2$ can be identified and distinguished from one another, because the main $Cu2p_{3/2}$ peak of CuO is around of 933.4–934 eV while that of $Cu(OH)_2$ is located at 934.5–935.3 eV [24,41,42]. Other Cu(II) compounds such as $Cu_3(PO_4)_2$ could be present overlapping the $Cu(OH)_2$ peak [40,41]. It has also been shown before that Cu(II) compounds present a shake-up peak typical of Cu(II) $d^9$ ions [43]. In the case of the copper spectra (Fig. 7a and b), the shake up peak at 944 eV is present, indicating a high content of Cu(II) compounds in the passive layer in both conditions. Table 4 presents the fitting results corresponding to the $Cu2p_{3/2}$ peaks. This fitting was carried out using XI SDP32 software. The peak areas were used to estimate the percentage of the different compounds present in the passive layer. The results presented in Table 4 show that on copper in IATW, Cu(II) compounds contribute in 93% to the global composition. Also, in IATW-BH, the participation of Cu(II) compounds is of nearly 81%.

**Table 4**
Deconvolution of $Cu2P_{3/2}$ peak. XI SDP32 software, version 3.0. FWHM (full width at half maximum).

| | Compound | Position (eV) | Peak | FWHM (eV) | Composition (atom %) |
|---|---|---|---|---|---|
| IATW | $Cu^0$, $Cu_2O$ | 932.5 | A | 1.6 | 7 |
| | CuO | 933.4 | B | 1.8 | 25 |
| | Cu(II) | 935.2 | C | 2.8 | 68 |
| IATW-BH | $Cu^0$, $Cu_2O$ | 932.5 | A | 2.6 | 19 |
| | CuO | 933.4 | B | 2.0 | 24 |
| | Cu(II) | 935.2 | C | 4.0 | 57 |

**Table 5**
Weight-loss measurements of copper coupons after 90 days of immersion.

| | ATW-BH | ATW | IATW | IATW-BH |
|---|---|---|---|---|
| Weight-loss (mg $cm^{-2}$) | 2.79 ± 0.38 | 0.43 ± 0.11 | 0.06 ± 0.03 | 0.21 ± 0.07 |
| Attack | General | General | None | None |

In summary, in the case of IATW-BH, XPS results show the participation of Cu(II) compounds on the passive layer, while Raman spectra show the incorporation of phosphate ions. As a result, the participation of $Cu_3(PO_4)_2$ is evident, which is in agreement with the results reported by other authors [9,14].

A mechanism to rationalize the situation of ATW and IATW has been proposed before [16]. When a passive layer grows on copper, the first step corresponds to the formation of $Cu(OH)_{ad.}$ Later, a $Cu_2O$ layer develops by dehydration. When $PO_4^{3-}$ ions are present, the Cu(I) solubility increases and the $Cu_2O$ layer formation can be partially inhibited. An upper layer of CuO can be formed by direct oxidation of $Cu_2O$ or by oxidation of $Cu^+$ ions previously dissolved from the surface. In any the case, the development of a protective passive layer could be better related to the presence of CuO [16,17,44,45].

In the presence of $PO_4^{3-}$ and NaClO the proposed mechanism needs to be modified. $Cu^+_{(aq)}$ could be oxidized by NaClO to $Cu^{2+}_{(aq)}$ (see Eq. (2)), hindering CuO formation.

$$2Cu^+_{(aq)} + ClO^- + H_2O \rightarrow 2Cu^{2+}_{(aq)} + Cl^- + 2\,OH^- \quad (2)$$

The increment in the concentration of $Cu^{2+}_{(aq)}$ would lead to the precipitation of $Cu_3(PO_4)_2$ ($pK = 37$) [44] as shown by Eq. (3), which would become a key component of the protective layer.

$$3Cu^{2+}_{(aq)} + 2PO_4^{3-}{}_{(aq)} \rightarrow Cu_3(PO_4)_2 \quad (3)$$

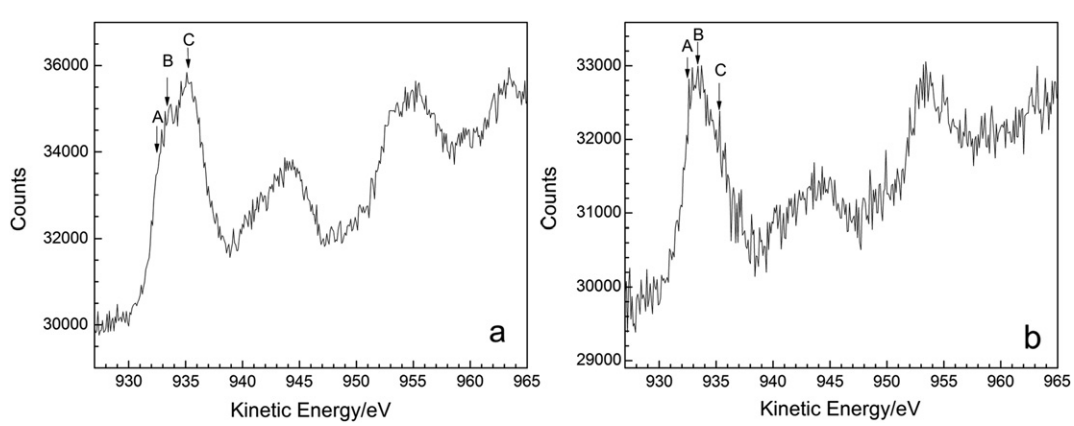


**Fig. 7.** XPS spectra for passive layers grown on copper for 192 h at $E_{corr}$. a) IATW; b) IATW-BH.

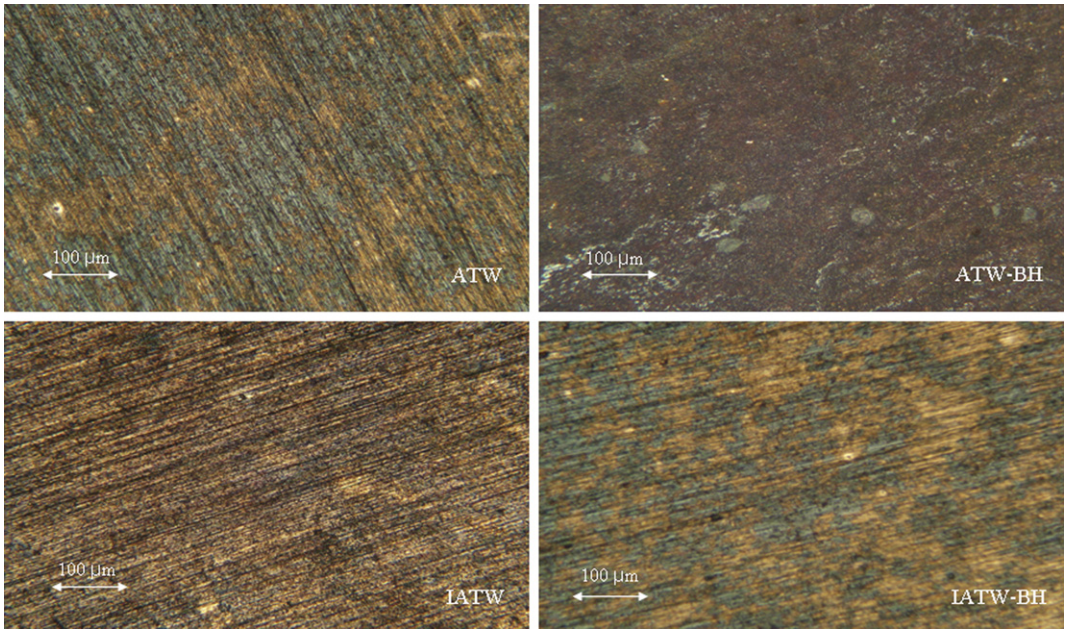


**Fig. 8.** Micrographs of coupons surface after 90 days of exposure.

To evaluate the performance of the inhibitor at even longer times, weight loss tests were carried out exposing copper coupons to ATW, IATW, ATW-BH and IATW-BH. Table 5 presents the weight-loss results after 90 days of exposure. Fig. 8 shows photographs of the coupons after removing them from each electrolyte and cleaning them as described before. No pitting attack was detected on the coupons under any of the conditions tested. However, after long immersion times, copper coupons undergo uniform dissolution in ATW-BH. Also, the weight loss is significant in ATW. When the inhibitor is added to ATW containing NaClO (IATW-BH), weight-loss is minimal, showing that general dissolution is inhibited.

The percentage of inhibition ($\eta_{R_p}$) can be calculated using the following equation, using $R_p$ values from Table 1:

$$\eta_{R_p} = \left[1 - \frac{R_{p\ \text{without inhibitor}}}{R_{p\ \text{with inhibitor}}}\right] \times 100 \quad (4)$$

It is also possible calculate the percentage of inhibition using Eq. (4) taking $R_{dl}$ from the impedance spectra in Table 2 ($\eta_{EIS}$). On the other hand, the percentages of inhibition using weight loss (WL) were calculated using the following equation:

$$\eta WL = \left[1 - \frac{m_{\text{with inhibitor}}}{m_{\text{without inhibitor}}}\right] \times 100 \quad (5)$$

where $m$ is the mass that has been lost. The percentages of inhibition are presented in Table 6. Those values calculated by means of WL are more likely to be accurate, taking into account the longer exposition times. Nevertheless, all the values presented in Table 6 are in good agreement, and demonstrate that phosphate ions are effective as corrosion inhibitor in the presence of NaClO.

**Table 6**
Inhibition percentages ($\eta$) for copper obtained from $R_p$ values, EIS and weight-loss tests.

| | IATW[a] | IATW-BH[b] |
|---|---|---|
| $\eta_{\text{weight-loss test}}$ | 86 | 92 |
| $\eta_{R_p}$ | 66 | 95 |
| $\eta_{EIS}$ | 77 | 94 |

[a] The blank condition corresponds to ATW.
[b] The blank conditions correspond to ATW-BL for $R_p$ and EIS measurements and to ATW-BH for the weight-loss test.

## 4. Conclusions

When a biocide agent such as NaClO is added to ATW the stability of the passive film, which in tap water is mainly composed by $Cu_2O$ [25], becomes compromised. Polarization resistance values decrease and $E_{corr}$ moves in the more active direction after the incorporation of NaClO. The polarization curves show a constant current increment, with no defined pitting potential, in agreement with the uniform dissolution observed at long immersion times.

The incorporation of phosphate ions as corrosion inhibitor produces a more compact and thinner surface layer, as compared to that in ATW. This layer is composed by a mixture of $Cu_2O$, CuO and $Cu(OH)_2$ [16,17]. This change in composition seems to be associated to a decrease in the copper cuprosolvency together with an increment in the pitting potential.

When the biocide and the inhibiting agent are both present, the passive layer on copper is thicker and more compact than in IATW. $E_{corr}$ moves towards more noble potentials accompanied by a noticeable increment in the $R_p$ values. Even though the increment in $E_{corr}$ may enhance the risk of localized corrosion initiation, it has to be taken into account that the difference ($E_{pit} - E_{corr}$) is twice that in ATW. The mass lost at longer times is minimal when compared to ATW contaminated with NaClO, showing that uniform dissolution is inhibited (inhibition values are closed to 90%). The simultaneous presence of phosphate and hypochlorite ions is associated to the participation of $Cu_3(PO_4)_2$ in the surface film, as demonstrated by XPS and Raman spectroscopy.

In summary, the results confirm that phosphate ions are effective as corrosion inhibitors on copper in contact with tap water, even when high dosages NaClO are employed as biocide.

## Acknowledgements

This work has been supported by the University of Mar del Plata (Grant 15/G225), as well as by the National Research Council

(CONICET, PIP0661) and the Agencia Nacional de Promoción Científica y Tecnológica (PICT 6-34112). L. Yohai wishes to thank CIC, Argentina, for her fellowship.

## References

[1] D. Atlas, J. Coombs, O.T. Zajicek, Water Res. 16 (1982) 693–698.
[2] N. Boulay, M. Edwards, Water Res. 35 (2001) 683–690.
[3] P.K.A. Hong, Y.Y. Macauley, Water Air Soil Pollut. 108 (1998). 457–471.
[4] H. Cong, J.R. Scully, J. Electrochem. Soc. 157 (2010) C200–C211.
[5] J.C. Rushing, M. Edwards, Corros. Sci. 46 (2004) 3069–3088.
[6] M.M. Critchley, N.J. Cromar, N.C. McClure, H.J. Fallowfield, J. Appl. Microbiol. 94 (2003) 501–507.
[7] M. Edwards, L. Hidmi, D. Gladwell, Corros. Sci. 44 (2002) 1057–1071.
[8] S.O. Pehkonen, A. Palit, X. Zhang, Corrosion 58 (2002) 156–165.
[9] Y. Zhe, S.O. Pehkonen, Water Sci. Technol. 49 (2004) 73–81.
[10] S. Li, L. Ni, C. Sun, L. Wang, Corros. Sci. 46 (2004) 137–145.
[11] N. Soussi, E. Triki, J. Mater. Sci. 42 (2007) 3259–3265.
[12] N. Souissi, E. Triki, Corros. Sci. 50 (2008) 231–241.
[13] D. Lytle, M.N. Nadagouda, Corros. Sci. 52 (2010) 1927–1938.
[14] B.R. Lewandowski, D.A. Lytle, J.C. Garno, Langmuir 26 (2010) 14671–14679.
[15] K. Goh, T. Lim, P. Chui, Corros. Sci. (2008) 918–927.
[16] M.B. Valcarce, M. Vázquez, Corros. Sci. 52 (2010) 1413–1420.
[17] L. Yohai, W.H. Schreiner, M. Vázquez, M.B. Valcarce, Appl. Surf. Sci. 257 (2011).
[18] L. Yohai, M. Vázquez, M.B. Valcarce, Corros. Sci. 53 (2011) 1130–1136.
[19] Código Alimentario Argentino, Capítulo XII, artículo 982, Bs. As., Argentina, Ley 18284.
[20] A.F. Cantor, J.K. Park, P. Vaiyavatjamai, J. Am. Water Works Assoc. 95 (2003) 112.
[21] APHA/AWWA/WEF, Standart Methods for Examination of Water and Wastemater, nineteenth ed., (1995). Washington DC, USA.
[22] Guidelines for drinking-water quality, Health Criteria and Other Supporting Information, second ed,, World Health Organization, Geneve, 1996.
[23] American Society of Testing and Materials, ASTM G61-86, Philadelphia, 1993.
[24] J.F. Moulder, W.F. Stickle, P.E. Sobol, K.D. Bomben, Handbook of X-ray Photoelectron Spectroscopy, Physical Electronics Inc., Minnesota, 1995.
[25] M.B. Valcarce, S.R. de Sanchez, M. Vazquez, Corros. Sci. 47 (2005) 795–809.
[26] M.B. Valcarce, S.R. de Sanchez, M. Vazquez, J. Mater. Sci. 41 (2006) 1999–2007.
[27] L.J. Aljinovic, S. Gudic, M. Smith, J. Appl. Electrochem. 30 (2000) 973–979.
[28] A. Palit, S. Pehkonen, Corros. Sci. 42 (2000) 1801–1822.
[29] J. Shim, J. Kim, Mater. Lett. 58 (2004) 2002–2006.
[30] Scribner Associates Inc., Z Plot for Windows (1998).
[31] M.E. Folquer, S.B. Ribotta, S.G. Real, L.M. Gassa, Corrosion 58 (2002) 240–247.
[32] V.S. Sastri, Corrosion Inhibitors, John Wiley and Ltd., West Sussex, England, 1998.
[33] J.C. Hamilton, J.C. Farmer, R.J. Anderson, J. Electrochem. Soc. 133 (1986) 739–745.
[34] G. Niaura, Electrochim. Acta 45 (2000) 3507–3519.
[35] I.M. Bell, R.J.H. Clark, P.J.G. Christopher, Raman Spectroscopic Library, UCL Chemistry Faculty of Mathematical and Physical Sciences (MAPS), 1998.
[36] A. Tomandl, M. Wolpers, K. Ogle, Corros. Sci. 46 (2004) 997–1011.
[37] R.L. Frost, Spectrochim. Acta Part. A 60 (2004) 1439–1445.
[38] R.L. Frost, T. Kloprogge, P.A. .Williams, W. Martens, T.E. Johnson, P. Leverett, Spectrochim. Acta Part. A 58 (2002) 2861–2868.
[39] H. Marchebois, S. Joiret, C. Savalla, J. Bernard, S. Touzain, Surf. Coat. Technol. 157 (2002) 151–161.
[40] Y. Feng, K.S. Siow, W.K. Teo, K.L. Tan, A.K. Hsieh, Corrosion 53 (1997) 546–555.
[41] Y. Feng, W.K. Teo, K.S. Siow, K.L. Tan, A.K. Hsieh, Corros. Sci. 38 (1996) 369–385.
[42] W. Xiao, S. Hong, Z. Tang, S. Seal, J.S. Taylor, Corros. Sci. 49 (2007) 449–468.
[43] M.C. Biesinger, B.P. Payne, B.R. Hart, A.P. Grosvenor, S. McIntryre, L.W.M. Lau, R.S.C. Smart, J. Phys. Conf. Ser. 100 (2008) 012025.
[44] M. Drogowska, L. Brossard, H. Ménard, J. Electrochem. Soc. 139 (1992) 2787–2793.
[45] M. Drogowska, L. Brossard, H. Menard, J. Appl. Electrochem. 24 (1994) 344–349.